INSTITUTE OF PHYSICS PUBLISHING MODELLING AND SIMULATION IN MATERIALS SCIENCE AND ENGINEERING

Modelling Simul. Mater. Sci. Eng. **12** (2004) 197–204 PII: S0965-0393(04)70548-3

Formation of bound states in expanded metal studied via path integral molecular dynamics

P A Deymier and Ki-Dong Oh

Department of Materials Science and Engineering, University of Arizona, Tucson, AZ 85721, USA

Received 7 October 2003
Published 7 January 2004
Online at stacks.iop.org/MSMSE/12/197 (DOI: 10.1088/0965-0393/12/2/001)

Abstract

The usefulness of the restricted path integral molecular dynamics method for the study of strongly correlated electrons is demonstrated by studying the formation of bound electronic states in a half-filled expanded three-dimensional hydrogenoid body-centred cubic lattice at finite temperature. Starting from a metallic state with one-component plasma character, we find that bound electrons form upon expansion of the lattice. The bound electrons are spatially localized with their centre for the motion of gyration located at ionic positions. The number of bound electrons increases monotonically with decreasing density.

1. Introduction

The study of strongly correlated electronic systems is one of the most challenging problems in condensed matter theory. Modelling and simulation have made great strides in the understanding of correlated electron gases [1–8]. The investigation of the behaviour of correlated electrons on crystalline lattices has also received a great deal of attention for its relevance to the metal to insulator transition (MIT) in several materials such as in transition metal oxides [9, 10]. The half-filled Hubbard model is widely accepted as a canonical model which can describe correlation effects [11]. Many approximate schemes have been employed to study the Hubbard model in various dimensions [12] yielding conflicting results as to the nature of a MIT [13]. The behaviour of correlated electrons on a lattice can be visualized simply by following Mott's original argument concerning the evolution of the electronic structure of an expanded hydrogenoid lattice [14]. In this simple model, Mott stressed the essential role of electron–electron interactions. For instance, the formation of electronic bound states at zero temperature depends on the screening of the Coulomb interaction. The evolution of an expanded metallic lattice towards an insulating state (with only bound states), as the crystal is enlarged, is believed to result from a reduction in screening of the interactions between the electrons and the ions. The potential energy that tends to localize electrons competes with the kinetic energy that favours their delocalization.

In this paper, we revisit Mott's original argument by investigating the correlated electronic structure of an expanded three-dimensional hydrogenoid body-centred cubic (bcc) crystal at finite temperature. This system will serve as a non-trivial model for testing the usefulness

of the restricted path integral molecular dynamics (RPIMD) method for the study of strongly correlated electronic systems [15–17]. The RPIMD is a recent quantum molecular dynamics method applicable to the simulation of many-fermion systems at finite temperature. This method accounts for exchange and correlation effects. We show that this approach includes the necessary physics for observing the formation of bound electronic states in a three-dimensional bcc crystal as it is expanded isothermally from a paramagnetic metal.

This paper is organized as follows. In section 2, we describe in some detail the application of the RPIMD to the simulation of a rigid hydrogenoid lattice. We pay some attention to the limitations of the approach. The results of our simulations are reported and analysed in section 3. Finally, conclusions are drawn in section 4. A brief discussion of some possible extensions of the RPIMD method is also given in that section.

2. Model and method

We use a recent quantum molecular dynamics method applicable to the simulation of many fermion systems at finite temperature. The RPIMD method was introduced elsewhere [15–17]. This method makes use of (a) the discretized path integral representation of quantum particles as closed necklaces of P classical particles (beads) with quantum exchange treated through crosslinking of the chains [18]; (b) the non-locality of crosslinking along the chains [19]; (c) the restricted path integral [20] to resolve the problem of negative weights to the partition function due to exchange of indistinguishable particles.

We consider a rigid lattice of hydrogenoid ions interacting with a spin unpolarized assembly of electrons. This system is modelled with the effective classical Hamiltonian:

$$H = \sum_{k=1}^{N_{\rm el}} \sum_{i=1}^{P} \frac{1}{2} m^* (\dot{r}_i^{(k)})^2 + \sum_{i=1}^{P} \sum_{k>l}^{N_{\rm el}} \sum_{l=1}^{N_{\rm el}-1} \frac{(-e)(-e/P)}{4\pi\varepsilon_0 |r_i^{(k)} - r_i^{(l)}|} + \sum_{i=1}^{P} \sum_{k=1}^{N_{\rm el}} \sum_{I=1}^{N_{\rm ion}} \frac{V_{\rm ps}(R_I - r_i^{(k)})}{P}$$
$$+ \sum_{k=1}^{N_{\rm el}} \sum_{i=1}^{P} {}^{*} \frac{m_{\rm e} P}{2\hbar^2\beta^2} (r_i^{(k)} - r_{i+1}^{(k)})^2 - \frac{1}{\beta} \sum_{s=\uparrow}^{\downarrow} \frac{\sum_{i=1}^{P} \sum_{j=1}^{P} \ln \det[E_{ij}] \theta_{ijs}^{+}}{\sum_{i=1}^{P} \sum_{j=1}^{P} \theta_{ijs}^{+}} \qquad (1)$$

Here, m^* is an arbitrary mass ($m^* = 1$ a.u.) defining an artificial kinetic energy for the dynamics of the electron necklace beads. The positions of the beads and of the ions are indicated by r and R, respectively. The second term in equation (1) accounts for the electron Coulomb interactions. This term is essential for the observation of bound states on an expanded lattice since electron localization is driven by the on-site electron–electron Coulomb repulsion. The ion–electron potential is denoted as $V_{\rm ps}$, and we use for simplicity an empty core local pseudopotential [16, 17] with a core radius $R_{\rm c} = 1.5$ Å. The fourth term is the effective harmonic potential for distinguishable quantum particles [21]. The cyclic condition on the summation over the beads is denoted by an '$*$'. Finally, the fifth term is an exchange potential for electrons with identical spin $s = \uparrow$ or $\downarrow$. The function θ_{ij}^{+} ensures the restriction of the path integral since it takes on the values 1 and 0 for paths with positive and negative $\det[E_{ij}]$, respectively. All the exchange effects are included in the matrix $[E_{ij}]$ whose elements are defined by $E_{ij}^{kl} = A_{ij}^{kl}/A_{ij}^{kk}$ with $A_{ij}^{kl} = \exp(-(m_{\rm e}P/2\beta\hbar^2)(r_i^{(k)} - r_j^{(l)})^2)$ where k and l label the electrons. The indices i and j label beads along necklaces, $m_{\rm e}$ stands for the electron mass and $\beta = 1/k_{\rm B}T$.

The simulation cell with edge length L contains 54 ions arranged on a bcc lattice (27 unit cells) and 54 non-polarized electrons ($N_{s=\uparrow} = 27$ and $N_{s=\downarrow} = 27$). Periodic boundary conditions (PBC) are applied. The long-range Coulomb potentials in equation (1) are replaced by a shorter-range potential of the form $(1/r)\mathrm{erfc}(\eta r)$ where $\eta = 5.741/L_0$ and $L_0 = 15$ Å.

Here, erfc stands for the complementary error function. This modification of the Coulomb potential should not affect the localization of electrons on lattice sites significantly since this behaviour is controlled by the on-site electron Coulomb potential which is essentially short-range. All potentials are truncated at $L/2$ to avoid artefacts associated with PBC (e.g. interactions between beads and their periodic images). The RPIMD is amenable to computer parallelization over the P beads.

Spin flip is not allowed in the model, i.e. the spin state is permanently attached to an electron. In the event of the formation of a local magnetic moment on a lattice site, change in polarization of this site may only occur by substitution of one electron with another one carrying an opposite spin. Therefore, long-range magnetic ordering would require collective transport of complete electron necklaces. Observation of long-range magnetic ordering with the RPIMD is, therefore, unlikely due to the long relaxation time associated with necklace diffusion. Additional frustration in magnetic ordering may also arise from the small difference in the distance between first and second nearest neighbours in the bcc lattice.

We solve the equations of motion with a leap-frog scheme and an integration time step of 2.8×10^{-16} s. We use $P = 400$ beads for the electron necklaces in order to ensure convergence of the path integral at the temperatures and densities studied [16, 17]. We eliminate all phonons by holding the ions at fixed positions. The temperature is maintained at a value for which the electrons are in a nearly degenerate regime at high density [16, 17]. It is known that the simulation of stiff harmonic chains suffers from non-ergodicity. To alleviate this problem, we couple every group of 54 beads (electrons) with identical label 'i' to a Nosé–Hoover chain of thermostats [22]. The chain length is equal to five. The first thermostat directly coupled to the electrons has a mass of 100 a.u. and the four other thermostats have a mass of 10 a.u. We have observed that this way of thermostating the electrons still yields non-ergodic behaviour for highly dilated crystals. To overcome this difficulty we have also coupled each necklace to an Andersen's thermostat [23]. This thermostat assigns velocities, distributed according to a Maxwell–Boltzmann distribution, to a necklace selected randomly every 50 integration steps. We calculate the electron kinetic energy with two different estimators [21, 24].

3. Results

In a first series of simulations (series I), the simulations are run sequentially from high density to low density, starting from a cell with $L = 16$ Å, and a randomly generated initial necklace configuration. L is increased by increments of 2 Å from 16 to 36 Å. Each simulation, other than the first one, uses as starting configuration the final equilibrated configuration from a preceding simulation. A second series of simulations (II) starts with a system equilibrated separately (from a paramagnetic metallic state) at $L = 30$ Å and expands the cell by an increment of 1 Å up to $L = 40$ Å. The simulations with $30 \leqslant L \leqslant 36$ Å in series II were run to verify that they sampled the same region of phase space as series I. The results for systems with $L \in [30,\ 36]$ Å are reported as averages over the simulations from both series. For arithmetic reasons, the simulations in series II with $L \geqslant 38$ Å were performed at the lower temperature of 1000 K. All the simulations reported lasted at least 30 000 time steps with most simulations lasting between 60 000 and 160 000 steps. Because of limits in computational resources, each simulation is a sequence of shorter runs of approximately 10 000–15 000 steps.

The electron kinetic energy as a function of L is reported in figure 1. We plot the values of the kinetic energy calculated with the two different energy estimators. These values agree well with each other. We also calculated the standard deviation from the set of average energies obtained from the short runs constituting each simulation. At high density (short L) the value

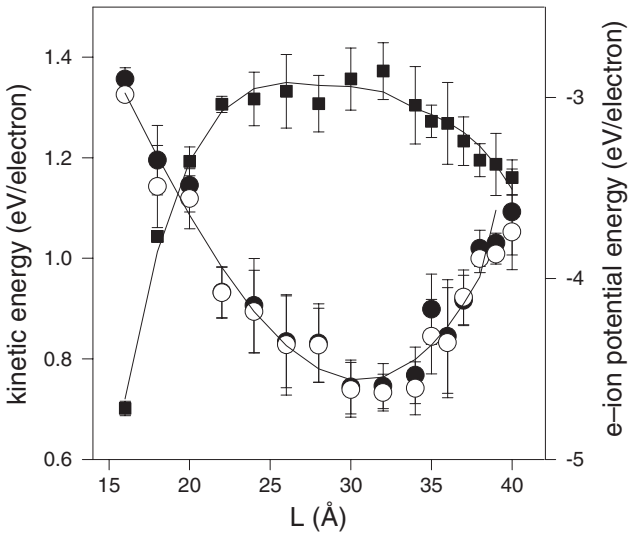

Figure 1. Average kinetic energies (○, ●) and electron–ion potential energy (■) versus cell size. The open and closed circles are calculated with the energy estimators of [22, 19]. The solid lines are guides to the eye.

of the kinetic energy approaches that of the electron plasma, i.e. ∼1.5 eV [3]. It decreases monotonically with decreasing density and reaches a minimum near $L = 32$ Å beyond which it increases. From $L = 16$–24 Å the density dependence of the kinetic energy is representative of the electron plasma [3]. The rise in kinetic energy at lower density is associated with the formation of compact electron necklaces, that is, electrons with highly localized wave functions. The electron–ion potential energy follows the opposite trend. The correlation energy (electron–electron Coulomb energy, not reported here) decays monotonically. In figure 2, we illustrate the evolution of the electronic structure upon expansion with distributions of the electrons' radius of gyration. The radius of gyration of an electron (k) is calculated using the following expression:

$$\mathrm{RG}^{(k)} = \frac{1}{P}\sqrt{\sum_{i=1}^{P}\left(r_i^{(k)} - \bar{r}^{(k)}\right)^2} \tag{2}$$

where $\bar{r}^{(k)}$ is the position of the centre of mass of the electron. At high densities, the distribution of the electrons' radius of gyration (RG) takes a nearly Gaussian form, characteristic of the electron plasma. Electrons are delocalized free carriers with a mean RG ∼ 4 Å. Although the PIMD method presented here, cannot be used to calculate directly a single particle excitation spectrum (i.e. a single particle density of states), the calculated distribution of RG suggests that the single particle excitation spectrum exhibits a single free carrier band as would be expected from a correlated metal. Compact electrons appear at an electron density $n = 6.75\,\text{Å}^{-3}$ ($L = 20$ Å) with a hydrogenoid radius $r_\mathrm{H} \sim 2$ Å. The compact electrons are in bound states since their centre of mass is located on ionic sites. The density at which we observe bound electrons is in good agreement with Mott's criterion for the formation of bound states: $n^{1/3} r_\mathrm{H} > 0.4$ [25]. Beyond 24 Å, the bound states form a narrow peak in the distributions of RG. The appearance of this peak is suggestive of a splitting of the single particle excitation spectrum. This observation is in accord with approximate numerical studies of the magnetically frustrated Hubbard model for lattices with infinite dimensions at half-filling, showing single

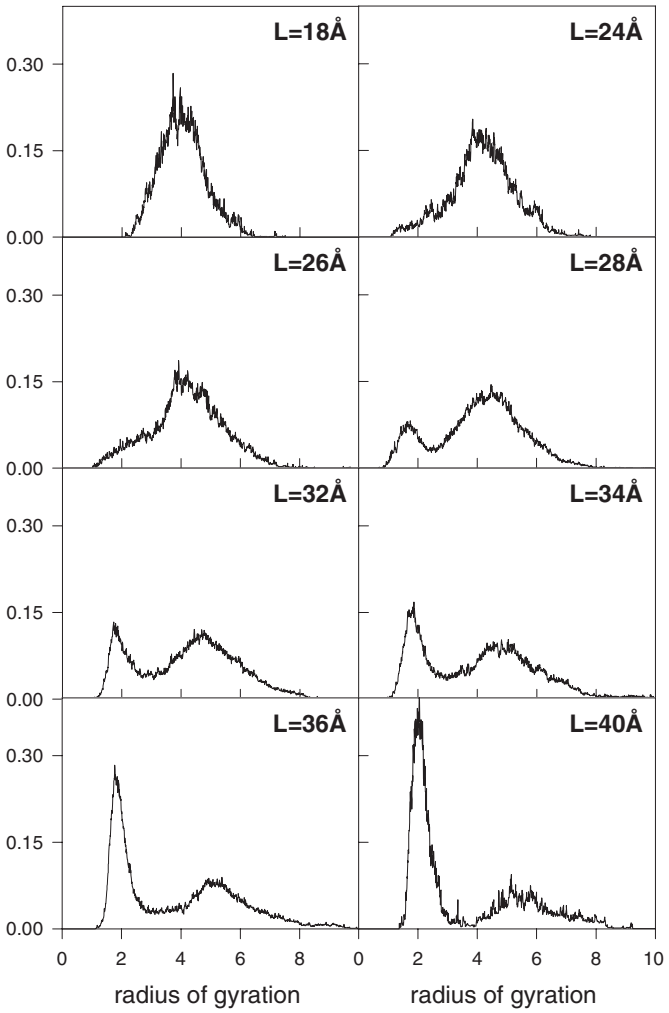

Figure 2. Distributions of electron radius of gyration (in Å) for several simulation cell sizes.

particle density of states that consist of a central free carrier band flanked by two Mott's sidebands [26, 27]. The bound electrons are in the sideband with lowest energy, the free carriers occupy part of the central band up to the Fermi energy. We estimate the number of bound electrons by integrating the RG distributions from 1 to 3 Å. The number of localized electrons increases with decreasing density. For $L = 24$ Å, 13.5% of the electrons are bound to a lattice site, whereas 63% of the electrons are in bound states for $L = 40$ Å. The loss of delocalized electrons results from a suppression of the free carrier broad peak in the RG distribution with only small changes in its width. This behaviour is indicative of a gradual build up of the spectral weight of the Mott's sidebands in the single particle excitation spectrum coupled with a suppression of the free carriers band. There is a change in the value of the free carrier's mean RG as expected from an increase in the inter-ionic distance. Since a free carrier hops between lattice sites, the spatial extent of its associated necklace depends on the distance between ionic sites. An equal number of bound electrons and free carriers are present near $L = 37$ Å. At very low densities ($L \geqslant 36$ Å), figure 2 shows the existence of electronic states with $8 < \mathrm{RG} < 10$ Å. These are electron necklaces extending over half the size of the

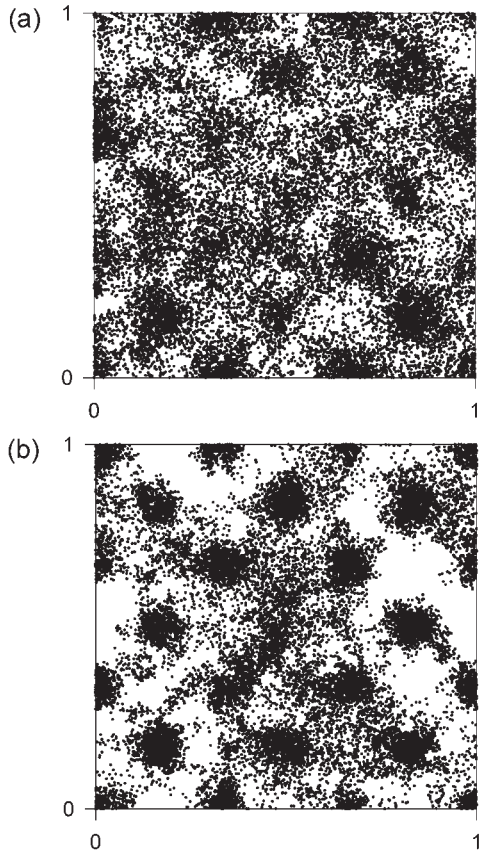

Figure 3. Snapshot projections of the position of the nodes of all the electron necklaces on the (100) plane of the bcc lattice for two densities. The simulation cell sizes are (*a*) $L = 24\,\text{Å}$ and (*b*) $L = 36\,\text{Å}$.

simulation cell. These electrons, however, represent a total of no more than a fraction of one electron. The rarity of highly extended electrons must result from their high energy. In terms of a single excitation spectrum, these electrons may be representative of the very few electrons that may, at finite temperature, occupy states in the Mott's upper band. It is worth noting that for the systems with $L < 40\,\text{Å}$, the bound electron and free carrier peaks are bridged by intermediate states. In the case of the system with $L = 40\,\text{Å}$, the RG distribution shows fewer intermediate states. This observation suggests an evolution of the excitation spectrum towards the opening of a gap between bound and free carrier excitations as the density becomes very low, i.e. a separation of the Mott's sidebands from the free carrier central band in the single particle excitation spectrum. The electronic structure of systems with very low density is currently inaccessible to us as our computer platform reaches its arithmetic limitations.

We have recorded the spatial arrangement of the bound electrons within the lattice. For $L \geqslant 26\,\text{Å}$ the bound electrons are not dispersed randomly throughout the cell but appear to cluster. At low overall electron density, the simulation cell is clearly inhomogeneous and divided into regions of high concentration of bound electrons and regions of high concentration of free carriers. These regions are in dynamical equilibrium. The coexistence of bound electrons and free carriers is illustrated in figure 3. Each dot in figure 3 represents a bead of an

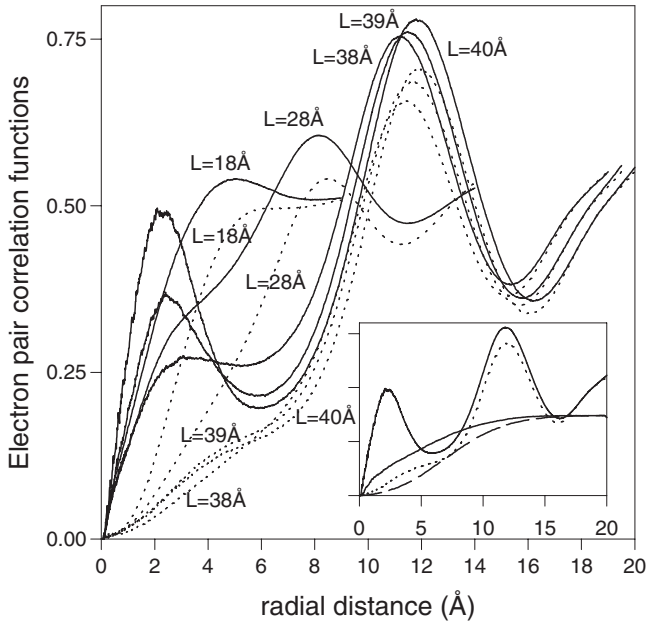

Figure 4. Heterospin (——) and isospin (· · · · · ·) electron PCFs for several values of L. The PCFs are truncated at $L/2$. Note that, in an unpolarized system, the total number of pairs of heterospin electrons exceeds that of isospin electrons. The inset represents the $L = 40$ Å PCFs and the renormalized electron plasma heterospin and isospin PCF (monotonically increasing solid and dashed lines).

electron necklace. Compact necklaces located on ionic sites correspond to bound electrons. The projection along the [100] direction of the bcc lattice is clearly outlined by the spatial distribution of the electrons' beads.

The change in the electronic structure of the expanded bcc lattice is also clearly seen in the heterospin, $g_{\uparrow\downarrow}$, and isospin, $g_{\uparrow\uparrow \text{ and } \downarrow\downarrow}$, electron pair correlation functions (PCFs) reported in figure 4. At high densities ($L = 18$ Å), the PCFs are characteristic of the electron plasma [6, 16, 17] with a correlation hole in the heterospin PCF and a wider exchange correlation hole in the isospin PCF. With decreasing density (up to $L = 38$ Å) the heterospin PCF possesses a shoulder at a radial distance $\sim$2 Å. This distance corresponds to doubly occupied lattice sites (i.e. singlet states or electrons in Mott's upper band). This shoulder converts into a peak for $L \geqslant 39$ Å indicating a spatial localization of at least one of the electrons participating in doubly occupied sites. We calculated the number of heterospin electrons involved in doubly occupied sites by integrating $g_{\uparrow\downarrow}(r)$ radially over the interval [0, 6 Å]. This number does not amount to more than a fraction of an electron, supporting the fact that two heterospin electrons located on the same site are not favoured energetically due to their Coulomb repulsion (second term in equation (1)). The isospin PCF shows a non-zero but even smaller number of doubly occupied sites (i.e. triplet states). Two electrons with identical spin are less likely to occupy the same lattice site than their heterospin counterparts due to the additional exchange repulsion (fifth term in equation (1)). Upon dilation of the lattice the increasing number of singly occupied lattice sites leads to a growing peak in the PCF encompassing both the nearest and the second-nearest neighbour distances of the bcc lattice ($(L/3)(\sqrt{3}/2)$ and $(L/3)$, respectively). Finally, we have superposed in the inset of figure 4 the PCFs for $L = 40$ Å and the PCFs of an electron plasma. The electron plasma PCFs [16] are renormalized to the number of free carrier electrons

in the $L = 40$ Å system determined previously from the RG distribution. This plot shows that the PCFs of the expanded system can be visualized semi-quantitatively as the superposition of peaks representing localized electrons and a free carrier background with electron plasma-like character.

4. Conclusion

We have used the RPIMD method to study the change in the electronic structure of a three-dimensional bcc hydrogenoid rigid crystal upon expansion of the lattice. Our results show that the RPIMD method possesses the necessary physics to model the behaviour of strongly correlated electrons in a lattice and, subsequently, the formation of bound electronic states. The RPIMD uses a position representation of the electrons and provides a good description of electrons that may change from delocalized to localized states. In its present form, RPIMD includes electron exchange, correlation and electron–ion interactions. This method also enables the calculation of important thermodynamics and structural quantities. The RPIMD method could be easily extended to include (a) ion dynamics for the study of strongly correlated electrons in the presence of phonons or (b) a system with finite magnetization (i.e. a spin-polarized system). We note that a spin-polarized system is more costly computationally than an unpolarized one since the calculation of the exchange term in equation (1) would require the computation of the determinant of an $N_{\rm el} \times N_{\rm el}$ matrix instead of the determinant of two $N_{\rm el}/2 \times N_{\rm el}/2$ matrices.

References

[1] Gell-Mann M and Bruekner K 1957 *Phys. Rev.* **106** 364
[2] Ceperley D M 1978 *Phys. Rev.* B **18** 3126
[3] Ceperley D M and Alder B J 1980 *Phys. Rev. Lett.* **45** 566
[4] Perrot F and Dharma-wardana M W C 1984 *Phys. Rev.* A **30** 2619
[5] Dandrea R G, Ashcroft N W and Carlsson A E 1986 *Phys. Rev.* B **34** 2097
[6] Ortiz G and Ballone P 1994 *Phys. Rev.* B **50** 1391
[7] Perrot F and Dharma-wardana M W C 2000 *Phys. Rev.* B **62** 16536
[8] Perrot F and Dharma-wardana M W C 2001 *Phys. Rev. Lett.* **87** 206404
[9] Arima T, Tokura Y and Torrance J B 1993 *Phys. Rev.* B **48** 17006
[10] Ahn J S, Bak J, Choi H S, Noh T W, Han J E, Bang Y, Cho J H and Jia Q X 1999 *Phys. Rev. Lett.* **82** 5321
[11] Hubbard J 1963 *Proc. R. Soc. Lond.* A **276** 238
[12] Gebhard F 1997 *The Mott Metal–Insulator Transition: Models and Methods* (Berlin: Springer)
[13] Kalinowski E and Gebhard F 2002 *J. Low Temp. Phys.* **126** 979
[14] Mott N F 1990 *Metal–Insulator Transitions* 2nd edn (London: Taylor and Francis)
[15] Ki-Dong Oh and Deymier P A 1998 *Phys. Rev.* B **58** 7577
[16] Ki-Dong Oh and Deymier P A 1998 *Phys. Rev. Lett.* **81** 3104
[17] Ki-Dong Oh and Deymier P A 1999 *Phys. Rev.* B **59** 11276
[18] Chandler D and Wolynes P G 1981 *J. Chem. Phys.* **74** 4078
[19] Hall R W 1988 *J. Chem. Phys.* **89** 4212
Hall R W 1989 *J. Chem. Phys.* **91** 1926
[20] Ceperley D M 1992 *Phys. Rev. Lett.* **69** 331
[21] Parrinello M and Rahman A 1984 *J. Chem. Phys.* **80** 860
[22] Marthyna G J and Klein M L 1992 *J. Chem. Phys.* **97** 2635
[23] Andersen H C 1980 *J. Chem. Phys.* **72** 2384
[24] Herman M F, Bruskin E J and Berne B J 1982 *J. Chem. Phys.* **76** 10
[25] Mott N F 1961 *Phil. Mag.* **6** 287
[26] Rozenberg M, Kotliar G and Zhang X Y 1994 *Phys. Rev.* B **49** 10181
[27] Kotliar G 2002 *J. Low Temp. Phys.* **126** 1009
[28] Schlipf J, Jarrell M, van Dongen P G J, Blumer N, Kehrein S, Pruschke Th and Vollhardt D 1999 *Phys. Rev. Lett.* **82** 4890